

Electronic Supplementary Information for

Ratiometric Colorimetric “Naked eye” Selective Detection of CN⁻ ions by Electron Deficient Ni(II) Porphyrins and their Reversibility Studies

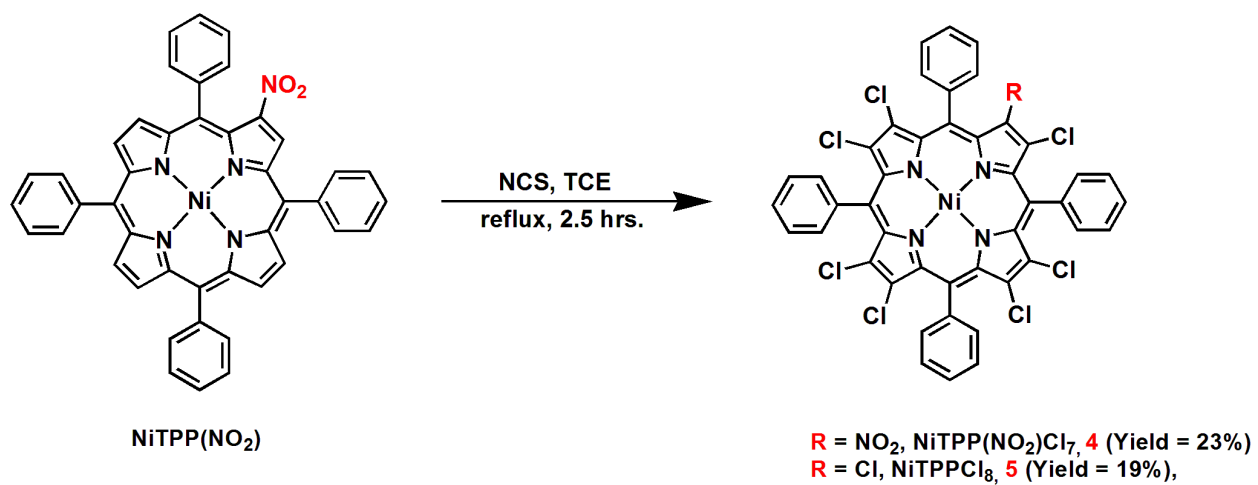
Ravi Kumar, Nivedita Chaudhri, and Muniappan Sankar*

Department of Chemistry, Indian Institute of Technology Roorkee, Roorkee – 247667, India

Table of Contents

	Page No
Scheme 1. Synthetic route to β -substituted electron deficient porphyrins (4,5)	3
Figure S1. UV-Vis absorption spectra of (a) 1 and 3 as well as (b) 4-5 in CH ₂ Cl ₂	4
Figure S2. ¹ H NMR spectrum of 1 in CDCl ₃ at 298 K	5
Figure S3. ¹ H NMR spectrum of 2 in CDCl ₃ at 298 K	5
Figure S4. ¹ H NMR spectrum of 3 in CDCl ₃ at 298 K	6
Figure S5. ORTEP diagrams showing top and side views of 3 (a-b), 4 (c-d) and 5 (e-f), respectively.	7
Figure S6. Colorimetric responses and corresponding absorption spectral changes of 2-5 while adding of excess of anions in toluene at 298 K.	11
Figure S7. UV-Vis spectral titrations of 2-5 with TBACN in toluene and insets show their corresponding Hill plots. The stoichiometry of 2-3 was established using Job's plot.	12
Figure S8. Ratiometric response of 2-5 on addition of 2 equiv. of cyanide ions in presence of 10 equiv. of other interfering anions. Blue bars indicate the references, Black bars indicate only with CN ⁻ ions, Green bars indicate various anions and red bar indicate the addition of cyanide ion in presence of interfering anions.	13
Figure S9. DPV traces of 2-5 in absence and presence of [CN ⁻] in CH ₂ Cl ₂ containing 0.1 M TBAPF ₆ at 298 K	14
Figure S10. UV-Vis spectra of 2-5 for complexation with 2CN ⁻ and reversibility test in toluene at 298 K, insets show corresponding colorimetric response for reversibility and reusability test.	15
Figure S11. Colorimetric response by coated paper strips of 2 and 3 (1 mM) with various anions in toluene (a, c) and neutral aqueous solution (b, d) at 298 K.	16
Figure S12. Colorimetric response by coated paper strips of 4 and 5 (1 mM) with various anions in toluene (a, c) and neutral aqueous solution (b, d) at 298 K.	17
Figure S13. B3LYP/LANL2DZ optimized geometry showing top (a) as well as side views (b) of NiTPP(NO ₂)Cl ₇ •2CN ⁻ , Hydrogens are omitted in both top and side views for clarity.	18
Figure S14. Pictorial representation of frontier molecular orbitals of NiTPP(CN) ₄ (1) obtained by DFT calculations using B3LYP as density functional with LANL2DZ basis sets in gas phase.	19

Figure S15. Pictorial representation of frontier molecular orbitals of NiTPP(CN) ₄ •2CN ⁻ (1 •2CN ⁻) obtained by DFT calculations using B3LYP as density functional with LANL2DZ basis sets in gas phase.	19
Figure S16. Pictorial representation of FMOs of NiTPP(NO ₂)Cl ₇ (4) obtained by DFT calculations using B3LYP as density functional with LANL2DZ basis sets in gas phase.	20
Figure S17. Pictorial representation of FMOs of NiTPP(NO ₂)Cl ₇ •2CN ⁻ (4 •2CN ⁻) obtained by DFT calculations using B3LYP as density functional with LANL2DZ basis sets in gas phase.	20
Figure S18. Theoretical UV-Visible spectra of (a) 1 and (b) 1 •2CN ⁻ obtained by TD-DFT calculations in gas phase.	21
Figure S19. Theoretical UV-Visible spectra of (a) 4 and (b) 4 •2CN ⁻ obtained by TD-DFT calculations in gas phase.	21
Figure S20. Single crystal X-ray structure of 3 with axial coordination of CN ⁻ . The counter cation (tetrabutylammonium ion) was not shown for clarity.	22
Figure S21. The time-dependent absorption changes of 1-5 after addition cyanide ions for 4 hours in toluene at 298 K.	23
Figure S22. MALDI-TOF negative ion mode mass spectrum of 1 in presence cyanide ions using HABA matrix.	24
Figure S23. UV-Visible spectra of (a) <i>meso</i> -tetraphenylporphyrinato nickel(II) (NiTPP); (b) <i>meso-tetrakis</i> (2,6-dichlorophenyl)porphyrinato nickel(II) (NiT(2,6-DCP)P); (c) 2,3,5,7,8,10,12,13,15,17,18,20-dodecaphenylporphyrinato nickel(II) (NiDPP); (d) 2,3,5,10,15,17,18,20-octaphenyl- porphyrinato nickel(II) (NiOPP); (e) <i>Meso-tetrakis</i> (<i>p</i> - ^t butylphenyl)porphyrinato nickel(II) (NiT(<i>p</i> - ^t bu-ph)P) in toluene (black lines) at 298 K and then excess addition of [CN ⁻] in toluene (red lines).	25
Figure S24. CVs of various planar and nonplanar Ni(II) porphyrins in CH ₂ Cl ₂ at 298 K.	26
Table S1. UV-Visible spectral data of 1-5 in CH ₂ Cl ₂ at 298 K.	4
Table S2. Crystal structure data of 1 (Py) ₂ (NiTPP(CN) ₄)(Py) ₂ , 3 (NiT(<i>p</i> -OMe-Ph)P(CN) ₄), 4 (NiTPP(NO ₂)Cl ₇), 5 (NiTPPCl ₈) and 3 •CN ⁻ (NiT(<i>p</i> -OMe-Ph)P(CN) ₄ (CN ⁻)).	8
Table S3. Selected average bond lengths and bond angles of 1 (Py) ₂ (NiTPP(CN) ₄)(Py) ₂ , 3 (NiT(<i>p</i> -OMe-Ph)P(CN) ₄), 4 (NiTPP(NO ₂)Cl ₇), 5 (NiTPPCl ₈) and 3 •CN ⁻ (NiT(<i>p</i> -OMe-Ph)P(CN) ₄ (CN ⁻)).	9
Table S4. Electrochemical redox data of 1- 5 in CH ₂ Cl ₂ at 298 K.	10
Table S5. Electrochemical redox data of various planar and nonplanar porphyrins in CH ₂ Cl ₂ at 298 K.	24



Scheme 1. Synthetic route to β -substituted electron deficient Ni(II) perhaloporphyrins (**4-5**).

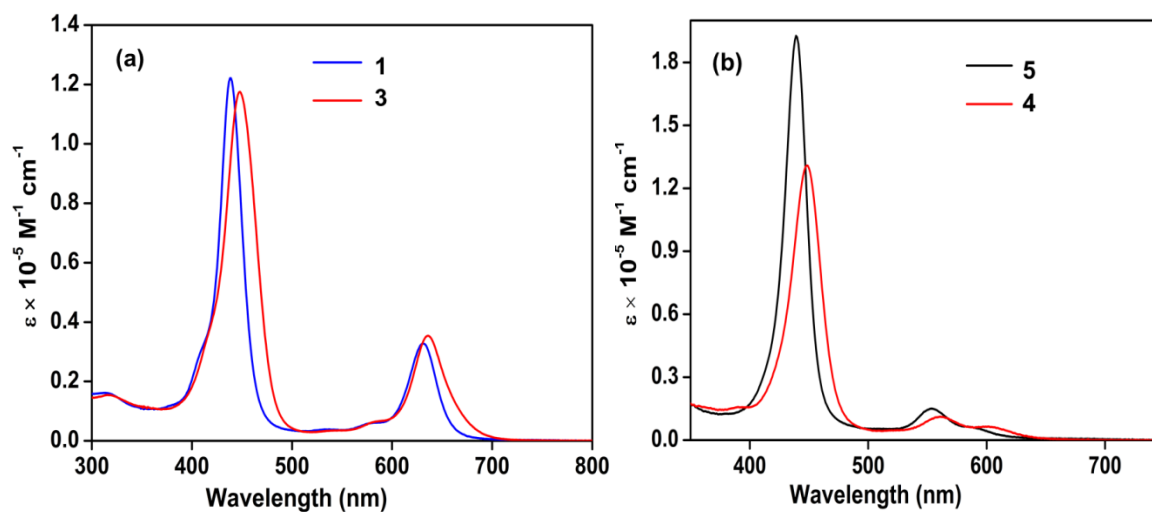


Figure S1. UV-Vis absorption spectra of (a) **1** and **3** as well as (b) **4-5** in CH_2Cl_2 at 298 K.

Table S1. UV-Visible spectral data of **1-5** in CH_2Cl_2 at 298 K.

Porphyrin	B band, nm	Q band(s), nm
1	440(5.10)	630(4.50)
2	445(5.13)	632(4.47)
3	450(5.07)	636(4.54)
4	448(5.12)	562(4.04), 604(3.80)
5	439(5.28)	554(4.18), 591(sh)

The values in parentheses refer to log ϵ .

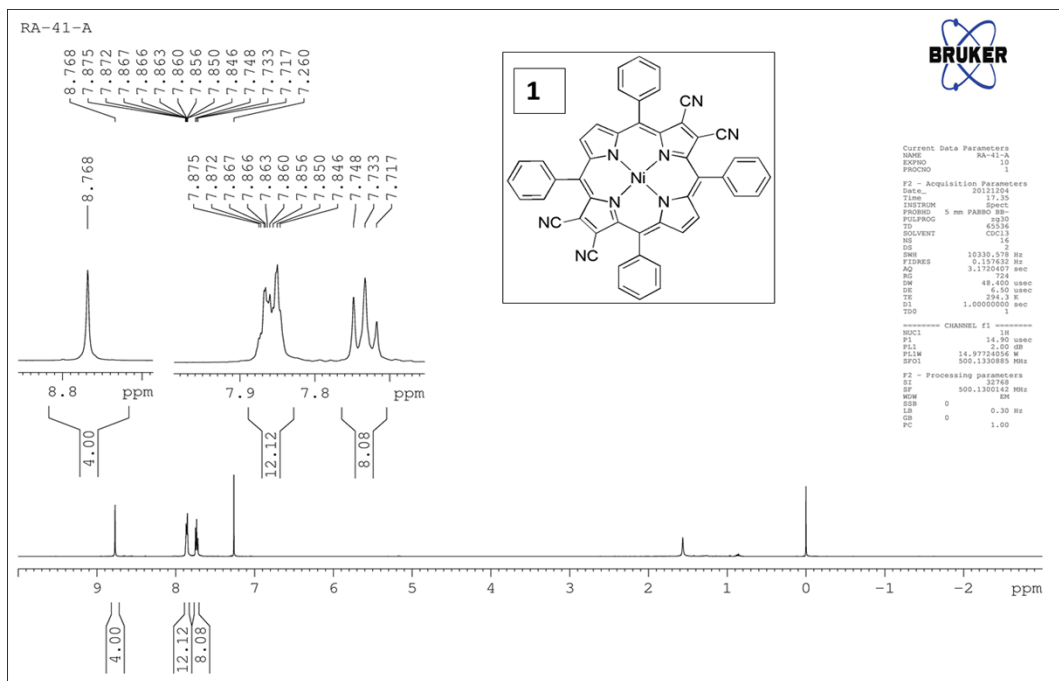


Figure S2. ^1H NMR spectrum of **1** in CDCl_3 at 298 K.

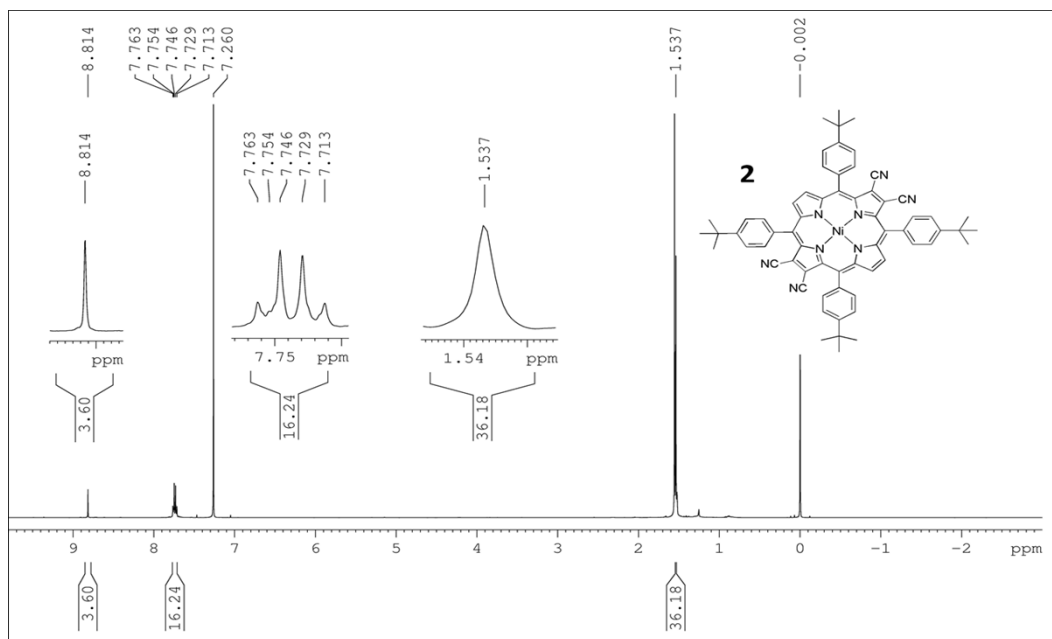


Figure S3. ^1H NMR spectrum of **2** in CDCl_3 at 298 K.

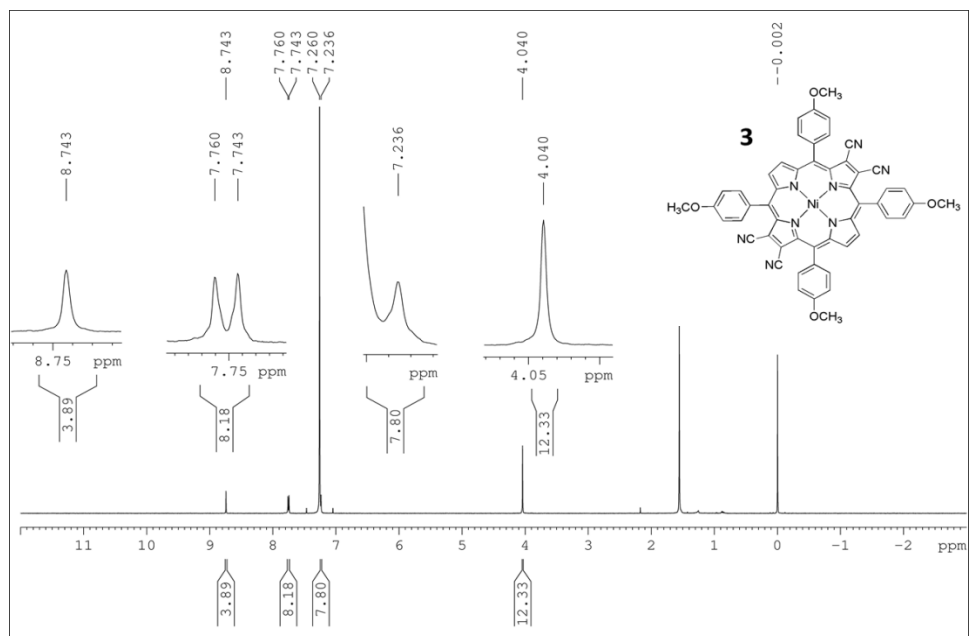


Figure S4. ^1H NMR spectrum of **3** in CDCl_3 at 298 K.

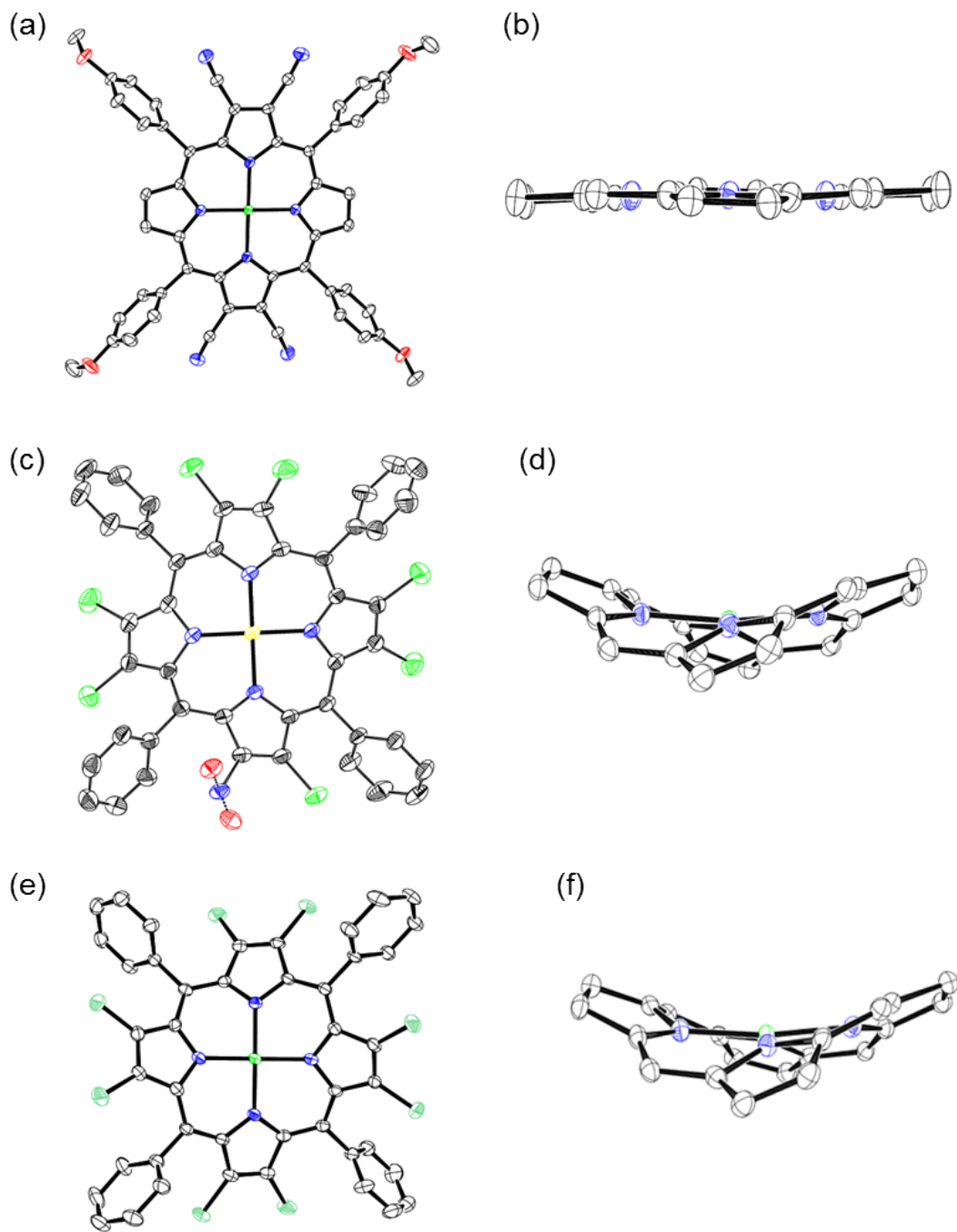
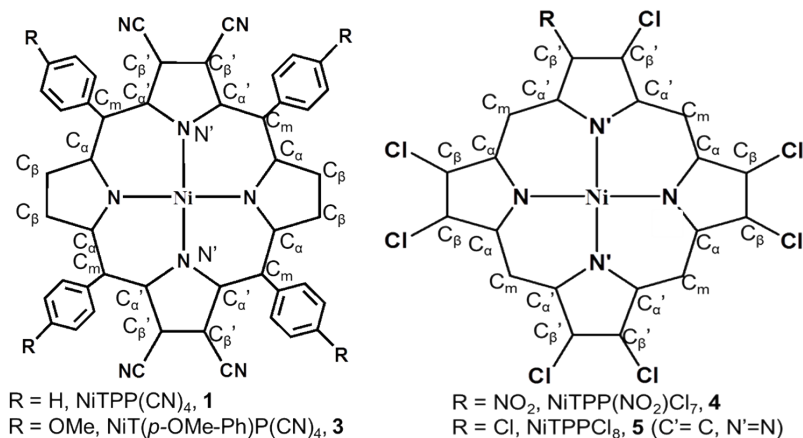


Figure S5. ORTEP diagrams showing top and side views of **3** (a-b), **4** (c-d) and **5** (e-f), respectively. Hydrogens are not shown for clarity, and in side views, the β -substituents and *meso*-phenyl groups are not shown for clarity.

Table S2. Crystal structure data of **1**(Py)₂ (NiTPP(CN)₄(Py)₂), **3** (NiT(*p*-OMe-Ph)P(CN)₄), **4** (NiTPP(NO₂)Cl₇), **5** (NiTPP(Cl)₈) and **3**•CN⁻ (NiT(*p*-OMe-Ph)P(CN)₄(CN⁻).

	1 (Py) ₂	3	4	5	3 •CN ⁻
Empirical Formula	C ₅₈ H ₃₄ N ₁₀ Ni	C ₅₂ H ₃₂ N ₈ NiO ₄	C ₄₄ H ₂₀ Cl ₇ N ₆ NiO _{0.5}	C ₄₄ H ₂₀ Cl ₈ N ₄ Ni	C ₆₉ H ₆₈ N ₁₀ NiO ₄
Formula wt.	929.66	891.56	947.52	946.95	1160.04
Crystal system	Triclinic	Monoclinic	Monoclinic	Monoclinic	Triclinic
Space group	P -1	C 2/c	P 21/c	P 21/c	P -1
<i>a</i> (Å)	9.340(5)	20.844(5)	14.4707(9)	14.5050(10)	14.154(5)
<i>b</i> (Å)	11.856(5)	10.732(5)	27.1087(15)	27.0592(17)	15.514(5)
<i>c</i> (Å)	13.471(5)	23.220(5)	10.8020(6)	10.7278(7)	16.154(5)
<i>α</i> (°)	87.223(5)	90.000(5)	90.00	90.00	61.669(5)
<i>β</i> (°)	70.308(5)	114.682(5)	110.527(2)	111.70	78.484(5)
<i>γ</i> (°)	68.356(5)	90.000(5)	90.00	90.00	86.358(5)
Volume (Å ³)	1300.5(10)	4720(3)	3968.4(4)	3912.1(4)	3057.4(17)
Z	1	4	4	4	2
ρ _{calc} (g/cm ³)	1.187	1.415	1.586	1.608	1.260
λ (Å)	0.71073	0.71073	0.71073	0.71073	0.71073
T (°C)	293 K	293 K	293 K	296 K	293 K
No. of total reflns.	6639	3699	9684	34311	25054
No. of indepnt. reflns.	6639	3699	9684	5467	4230
R	0.0418	0.0642	0.0534	0.0421	0.0437
R _w	0.1178	0.1952	0.1498	0.0910	0.1058
GOOF	1.024	1.074	1.046	0.896	1.043
CCDC No	1043611	1043609	1043615	1044025	1043610

Table S3. Selected average bond lengths and bond angles of **1**(Py)₂ (NiTPP(CN)₄)(Py)₂, **3** (NiT(*p*-OMe-Ph)P(CN)₄), **4** (NiTPP(NO₂)Cl₇), **5** (NiTPP(Cl)₈) and **3**•CN⁻ (NiT(*p*-OMe-Ph)P(CN)₄(CN⁻).



	1 (Py) ₂	3	4	5	3 .CN ⁻
Bond Lengths (Å ^o)					
Ni -N	2.035(16)	1.949(3)	1.906(2)	1.907(3)	2.039(4)
Ni -N'	2.074(16)	1.971(3)	1.912(2)	-	2.062(4)
N -C _α	1.370(2)	1.381(5)	1.382(4)	1.383(5)	1.373(6)
N' -C _α '	1.373(2)	1.390(5)	1.376(4)	-	1.374(6)
C _α -C _β	1.452(2)	1.430(6)	1.447(4)	1.445(6)	1.439(7)
C _α ' -C _β '	1.450(2)	1.429(5)	1.447(4)	-	1.434(7)
C _β -C _β	1.337(3)	1.323(6)	1.347(8)	1.354(5)	1.328(7)
C _β ' -C _β '	1.378(2)	1.362(5)	1.346(5)	-	1.366(7)
C _α -C _m	1.398(2)	1.384(5)	1.393(4)	1.393(6)	1.383(7)
C _α ' -C _m	1.409(3)	1.387(6)	1.395(4)	-	1.409(7)
ΔC_β^a	0.0721	0.059	0.871	0.898	0.184
Δ24^b	0.0604	0.0473	0.525	0.535	0.113
ΔNi	0.000	0.000	0.004	0.001	0.309
Bond Angles (°)					
N - Ni -N	180(0)	180.0(1)	172.3(10)	171.4(13)	160.9(15)
N' - Ni -N'	180(0)	180.0(1)	171.5(10)	-	164.8(15)
Ni -N -C _α	126.7(12)	128.1(2)	125.6(11)	125.5(3)	126.5(4)
Ni -N' -C _α '	125.8(12)	127.3(2)	125.4(10)	-	125.7(4)
N - C _α -C _m	126.6(15)	126.4(3)	123.9(4)	123.8(6)	126.5(7)
N' -C _α ' -C _m	125.6(16)	125.8(3)	124.1(4)	-	125.3(6)
N -C _α -C _β	109.4(15)	110.8(3)	108.4(3)	108.4(4)	109.3(5)
N' -C _α ' -C _β '	109.0(15)	110.0(3)	108.3(3)	-	109.2(5)
C _β -C _α -C _m	123.9(16)	122.8(4)	127.0(3)	127.0(4)	124.2(6)
C _β ' -C _α ' -C _m	125.4(16)	124.2(4)	126.8(3)	-	125.5(7)
C _α -C _β -C _β	107.3(2)	107.3(4)	107.6(3)	107.5(4)	107.6(5)
C _α ' -C _β ' -C _β '	106.9(15)	107.2(3)	107.5(3)	-	107.2(5)
C _α -N -C _α	106.6(13)	103.8(3)	107.1(2)	107.3(4)	106.3(4)
C _α ' -N' -C _α '	108.1(14)	105.3(3)	107.6(2)	-	107.2(4)
C _α -C _m -C _α	124.9(16)	122.3(4)	120.0(3)	120.1(4)	124.5(5)

^aΔC_β refers mean plane deviation of β-carbon atoms, ^bΔ24 refers mean plane deviation of 24 core atoms

Table S4. Electrochemical redox potentials^a of **1-5** in CH₂Cl₂ at 298 K.

Porphyrin	Oxidation(volts)	Reduction(volts)		$\Delta E_{1/2} (I_{ox}-I_{red})$ (Volts)
	I	I	II	
1	1.44	-0.38	-0.81	1.82
2	1.40	-0.44	-0.84	1.84
3	1.32	-0.43	-0.85	1.75
4	1.33	-0.64	-0.88	1.97
5	1.26	-0.82	-1.14	2.08

^avs Ag/AgCl

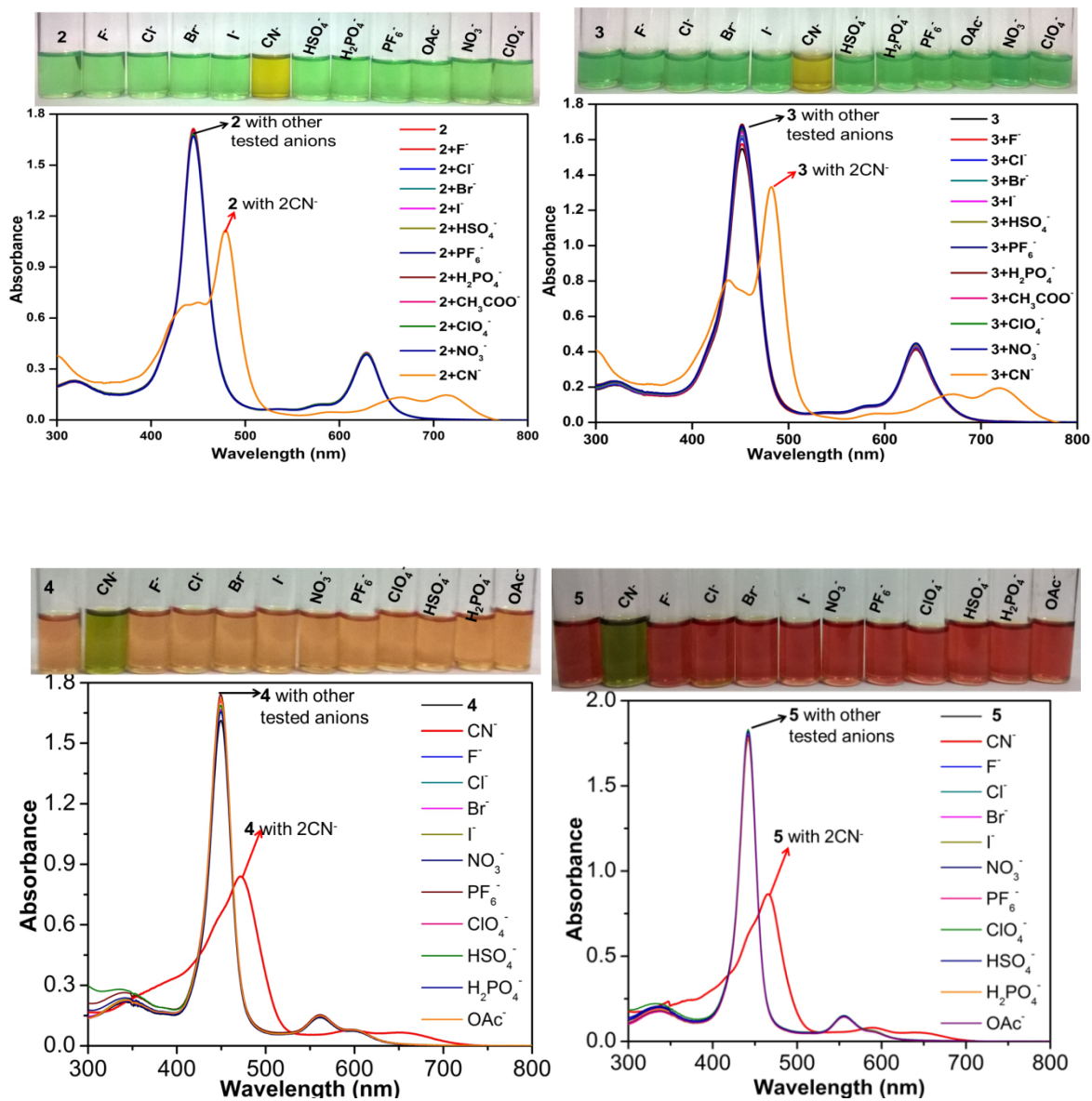


Figure S6. Colorimetric responses and corresponding absorption spectral changes of 2-5 while adding of excess of anions in toluene at 298 K.

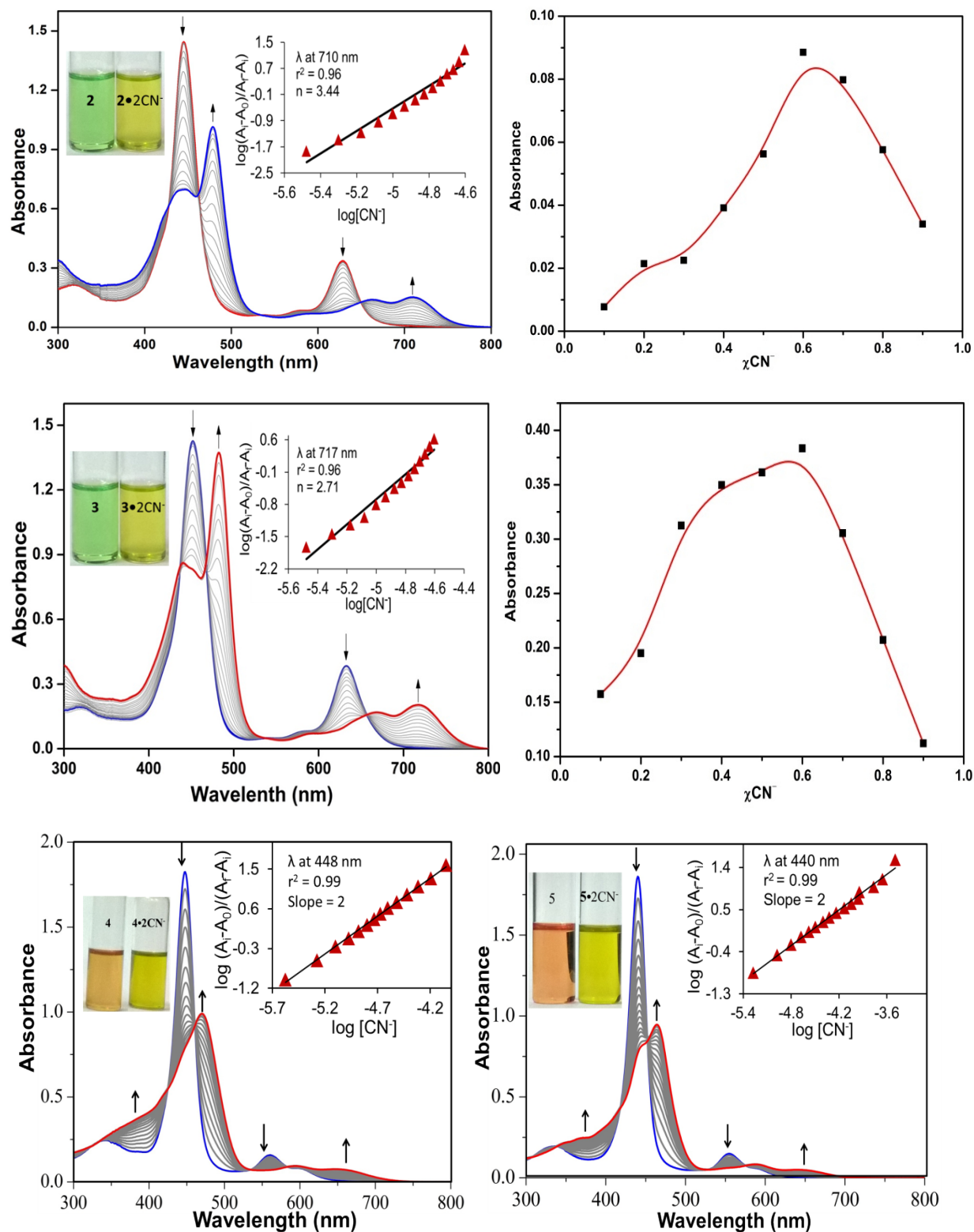


Figure S7. UV-Vis spectral titrations of **2-5** with TBCN in toluene and insets show their corresponding Hill plots. The stoichiometry of **2-3** was established using Job's plot.

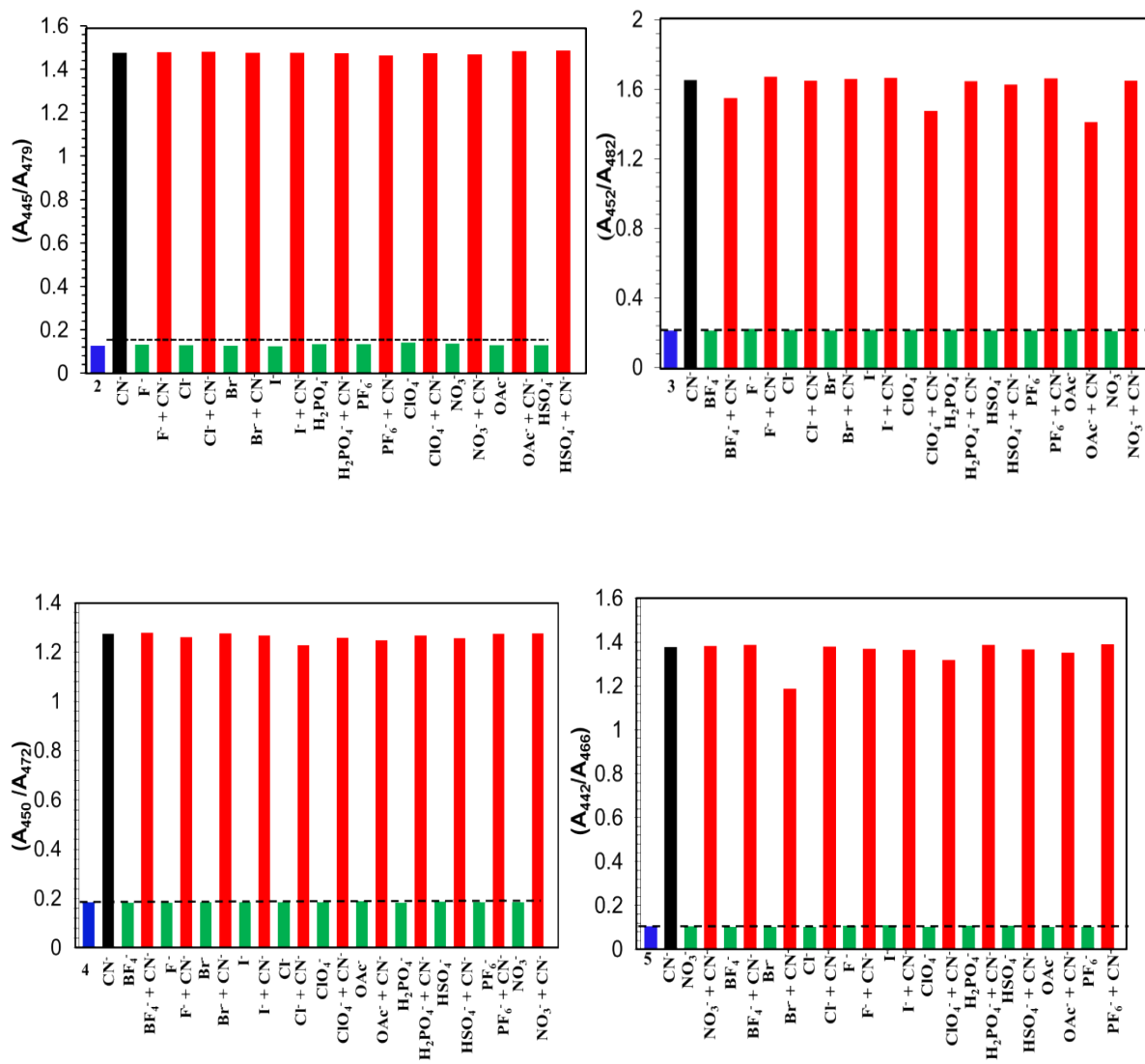


Figure S8. Ratiometric response of **2-5** on addition of 2 equiv. of cyanide ions in presence of 10 equiv. of other interfering anions. Blue bars indicate the references, Black bars indicate only with CN⁻ ions, Green bars indicate various anions and red bar indicate the addition of cyanide ion in presence of interfering anions.

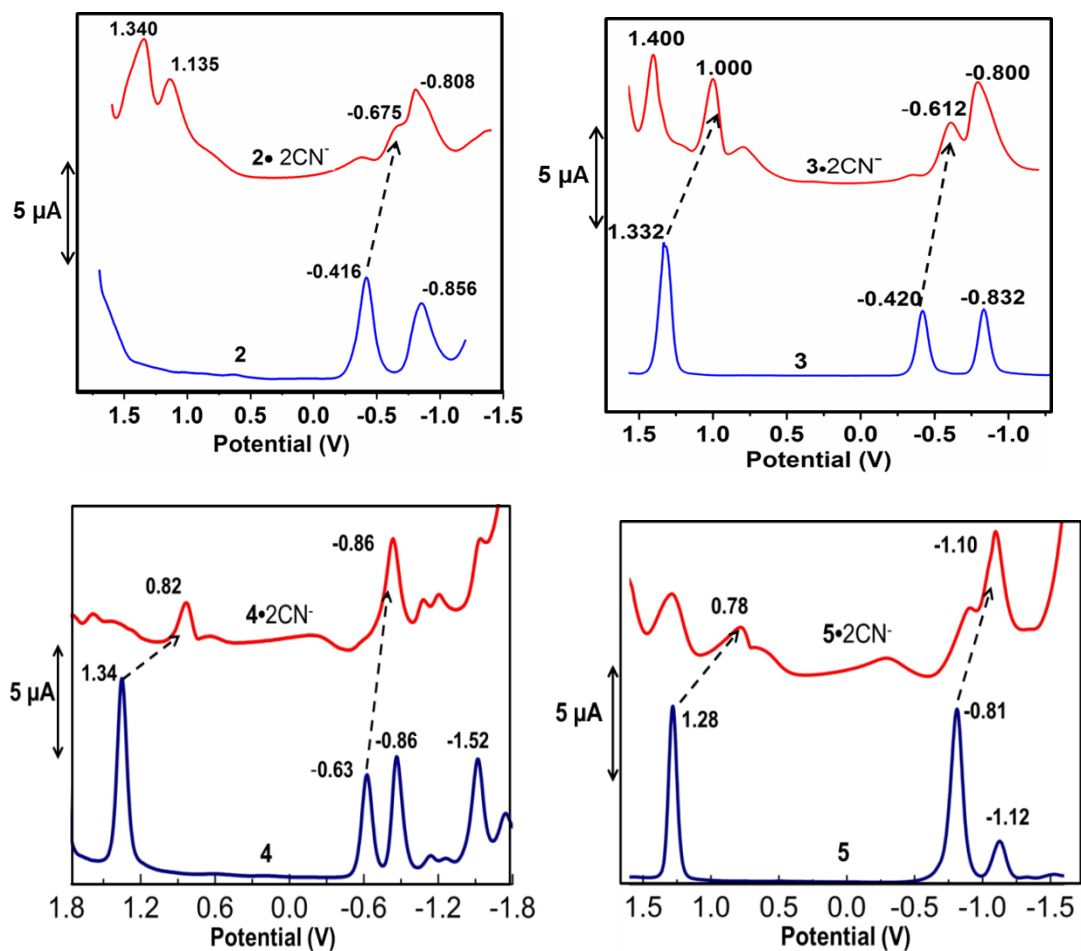


Figure S9. DPV traces of **2-5** in absence and presence of $[\text{CN}^-]$ in CH_2Cl_2 containing 0.1 M TBAPF_6 at 298 K.

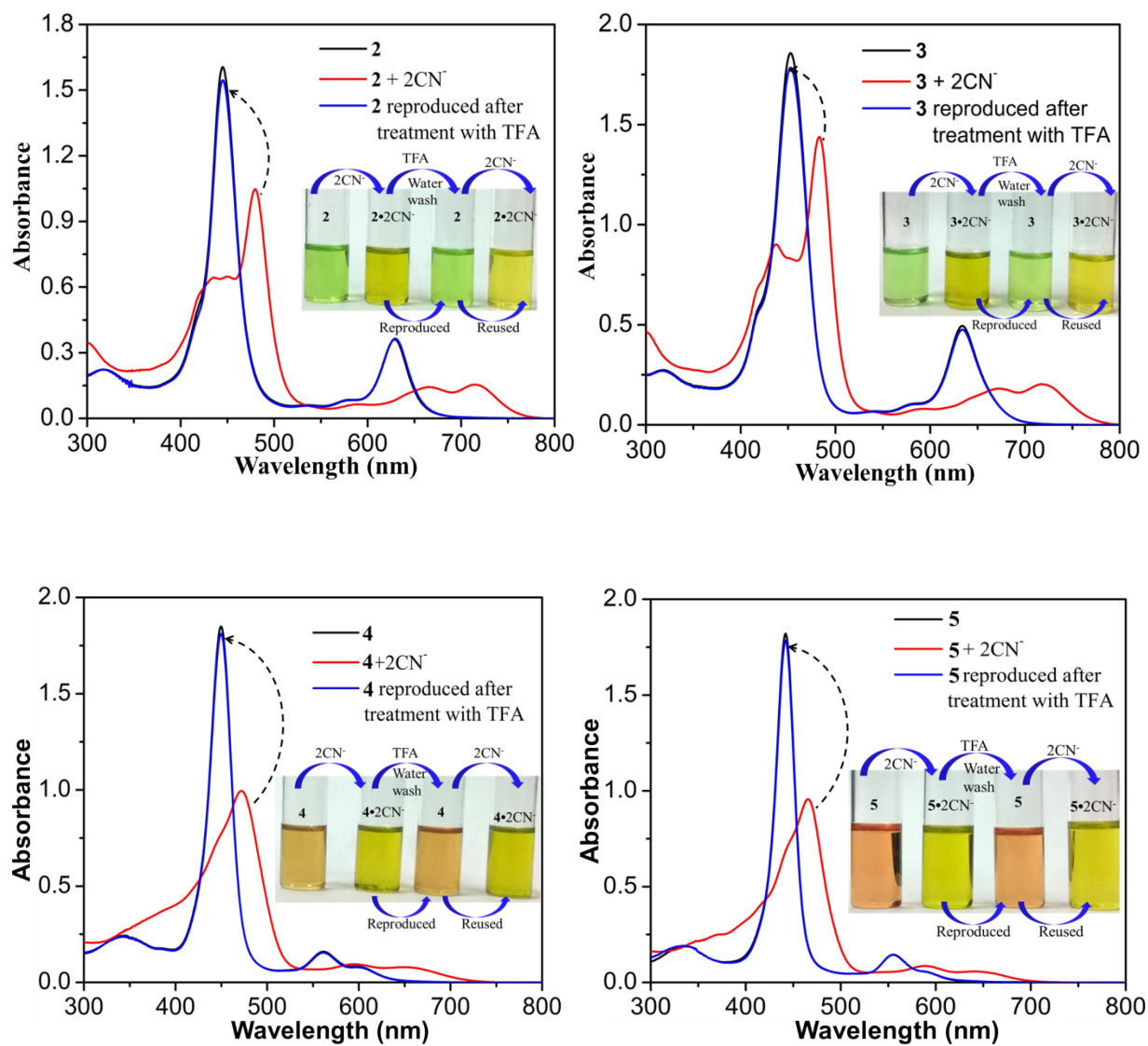


Figure S10. UV-Vis spectra of 2-5 for complexation with 2CN^- and reversibility test in toluene at 298 K, insets show corresponding colorimetric response for reversibility and reusability test.

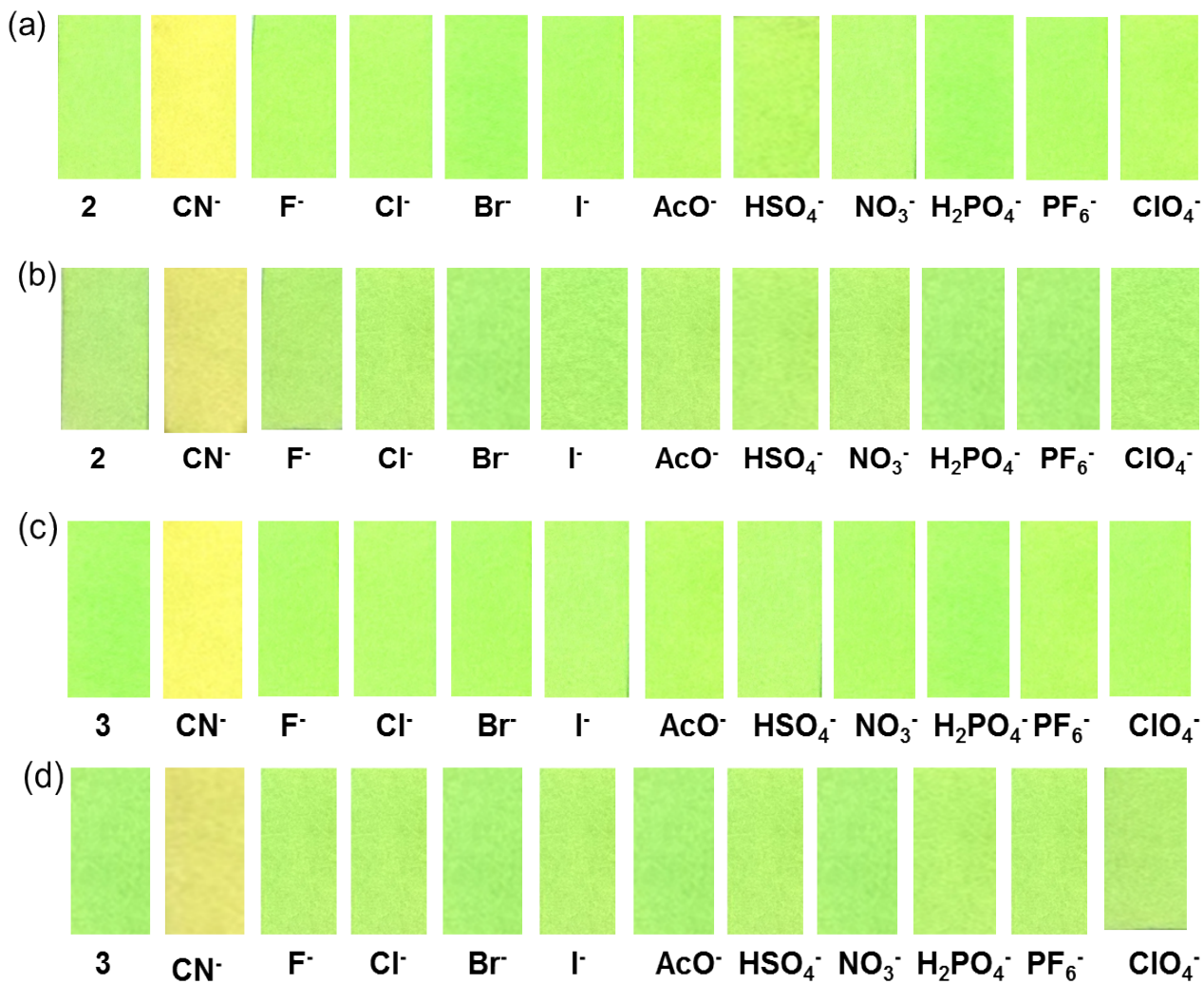


Figure S11. Colorimetric response by coated paper strips of **2** and **3** (1 mM) with various anions in toluene (a and c) and neutral aqueous solution (b and d) at 298 K.

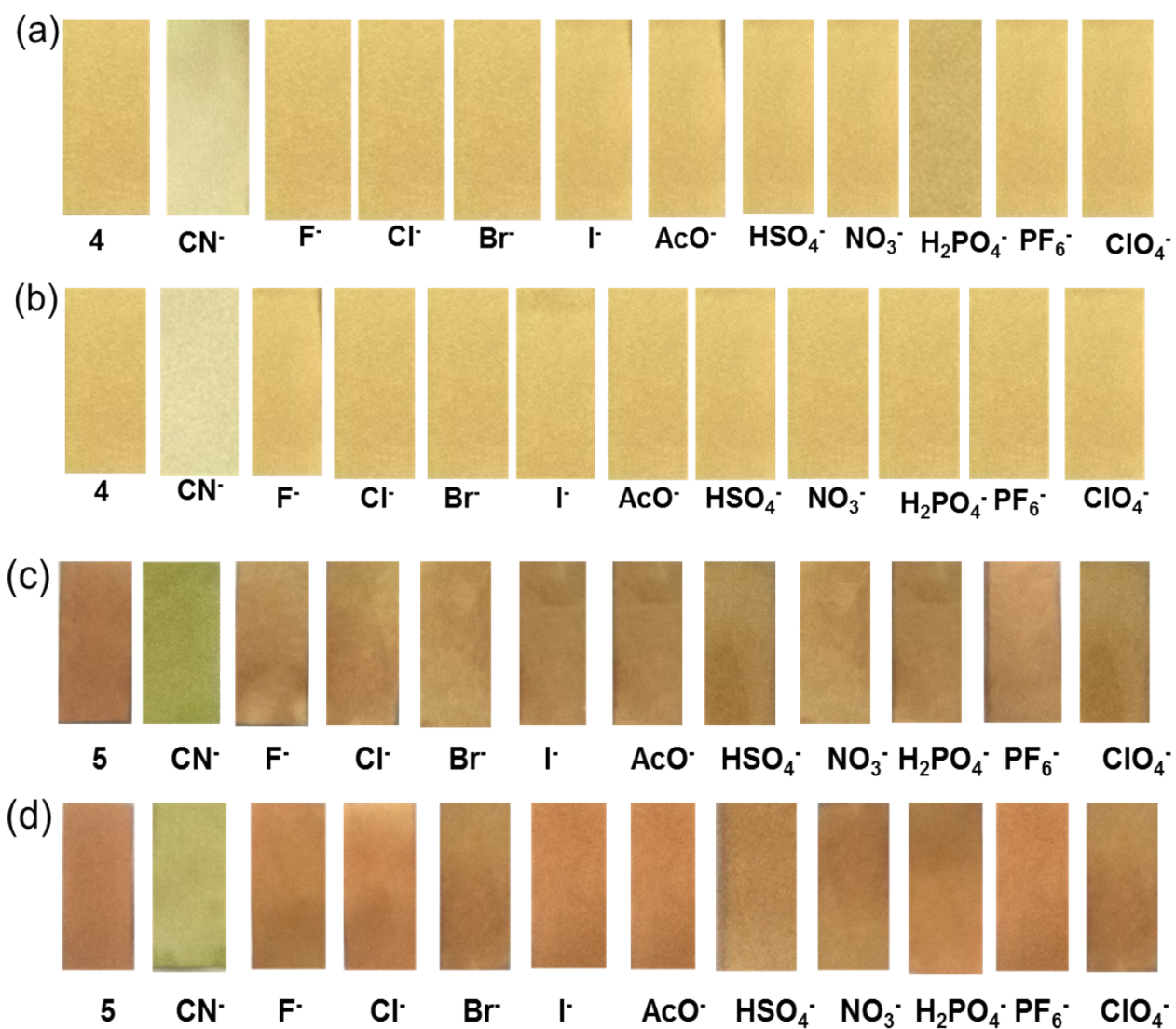


Figure S12. Colorimetric response by coated paper strips of 4 and 5 (1 mM) with various anions in toluene (a,c) and neutral aqueous solution (b,d) at 298 K.

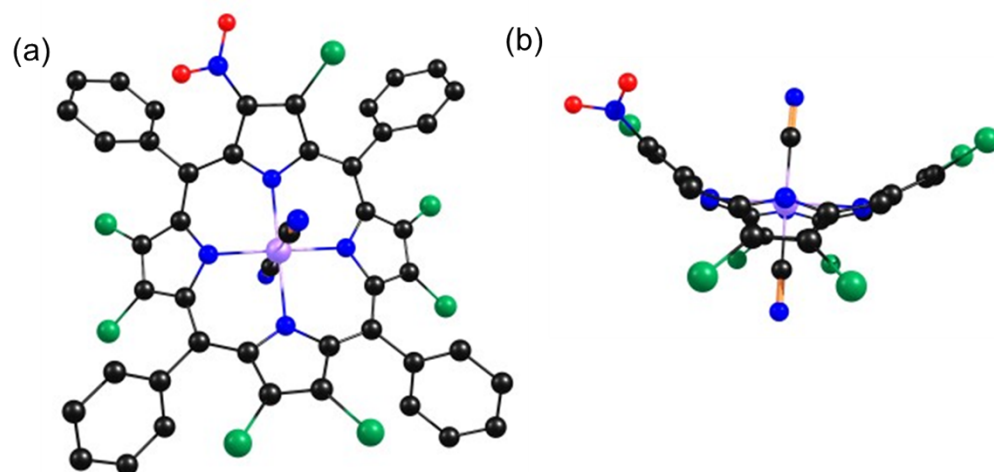


Figure S13. B3LYP/LANL2DZ optimized geometry showing top (a) as well as side views (b) of $\text{NiTPP}(\text{NO}_2)\text{Cl}_7 \cdot 2\text{CN}^-$, hydrogens are omitted in both top and side views for clarity.

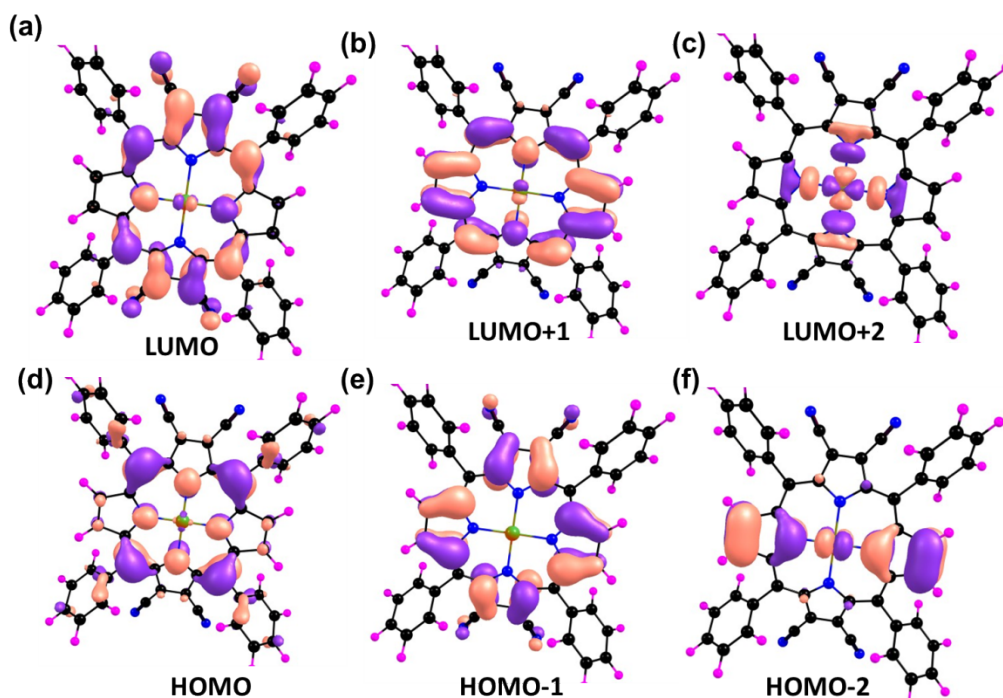


Figure S14. Pictorial representation of frontier molecular orbitals of NiTPP(CN)₄ (1) obtained by DFT calculations using B3LYP as density functional with LANL2DZ basis sets in gas phase.

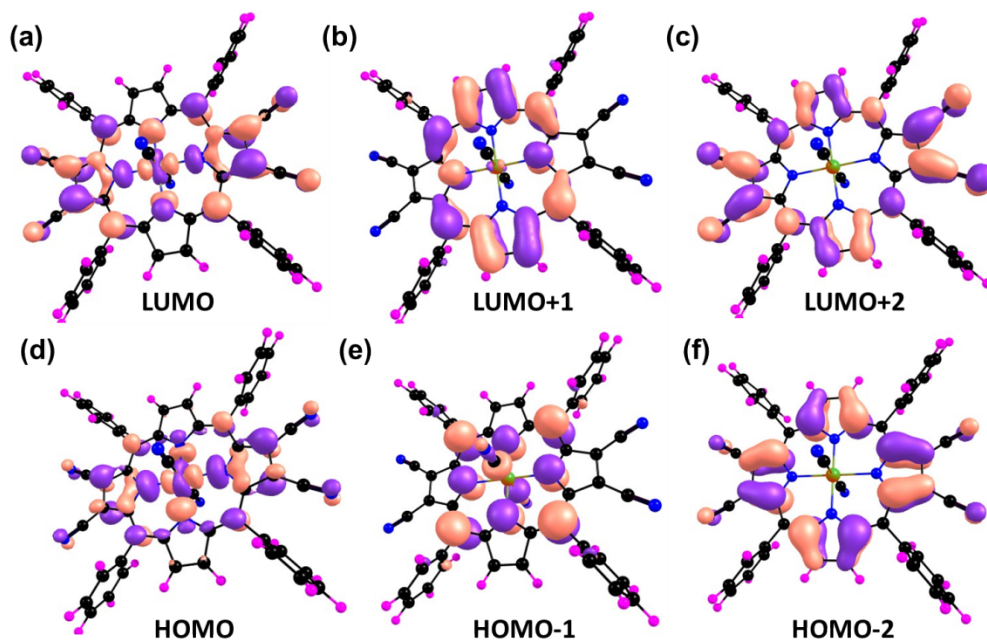


Figure S15. Pictorial representation of frontier molecular orbitals of NiTPP(CN)₄•2CN⁻ (1•2CN⁻) obtained by DFT calculations using B3LYP as density functional with LANL2DZ basis sets in gas phase.

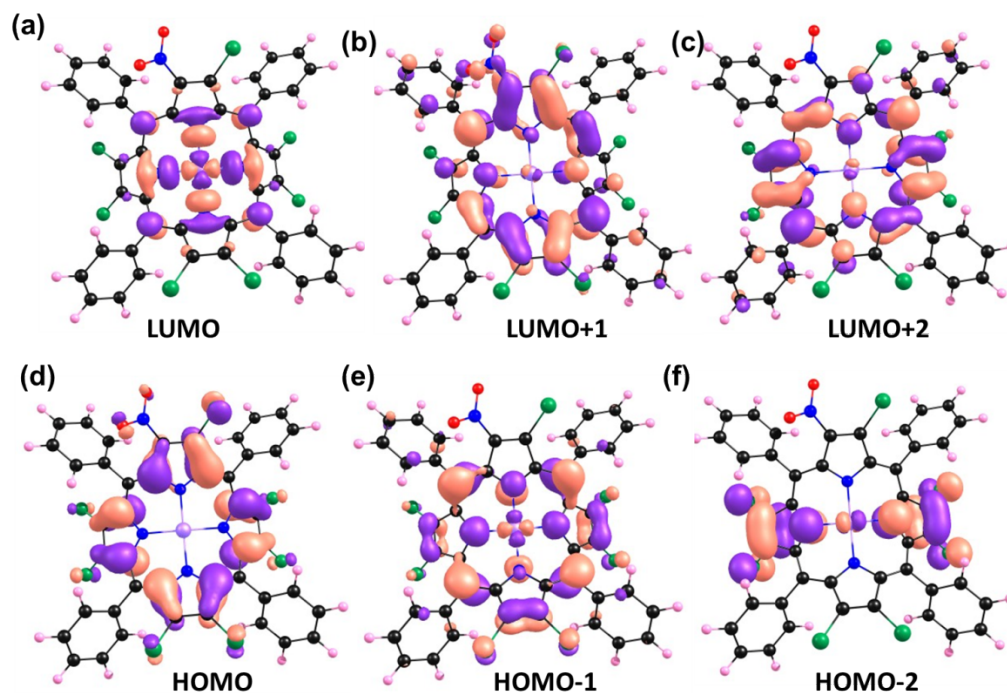


Figure S16. Pictorial representation of frontier molecular orbitals of NiTPP(NO₂)Cl₇ (**4**) obtained by DFT calculations using B3LYP as density functional with LANL2DZ basis sets in gas phase.

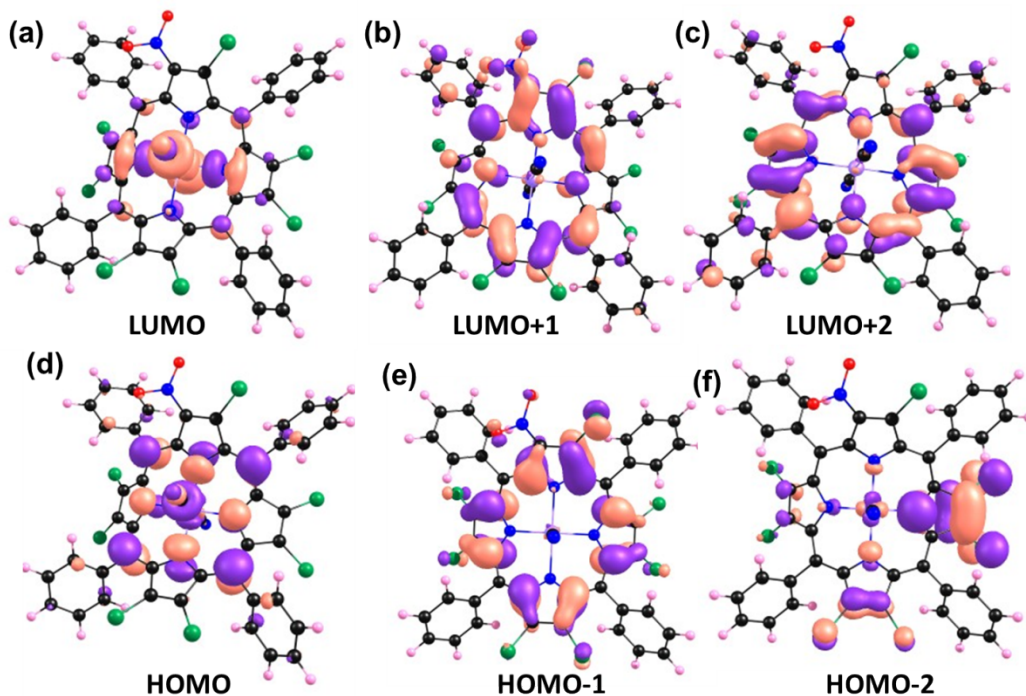


Figure S17. Pictorial representation of frontier molecular orbitals of NiTPP(NO₂)Cl₇•2CN⁻ (**4**•2CN⁻) obtained by DFT calculations using B3LYP as density functional with LANL2DZ basis sets in gas phase.

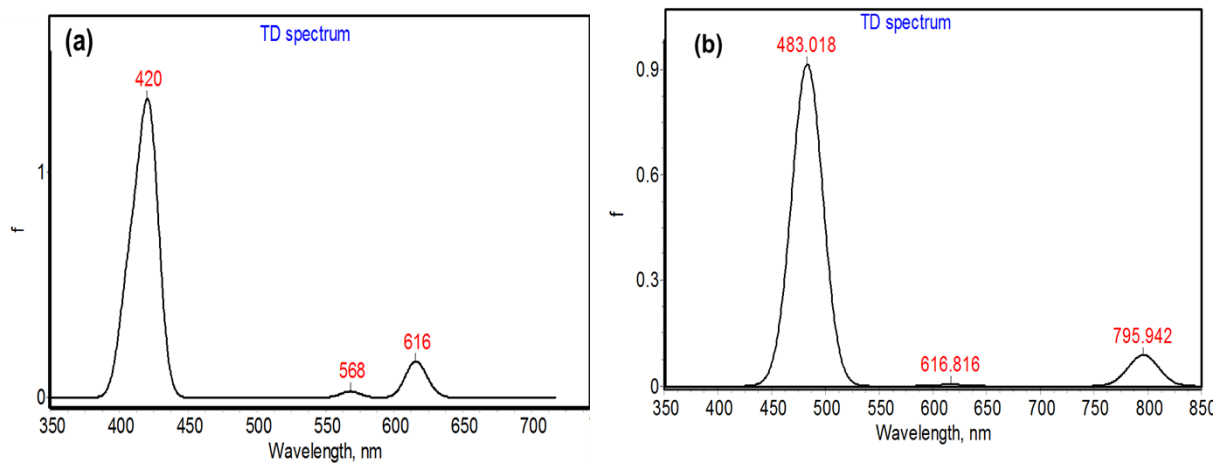


Figure S18. Theoretical UV-Visible spectra of (a) **1** and (b) **1•2CN⁻** obtained by TD-DFT calculations in gas phase.

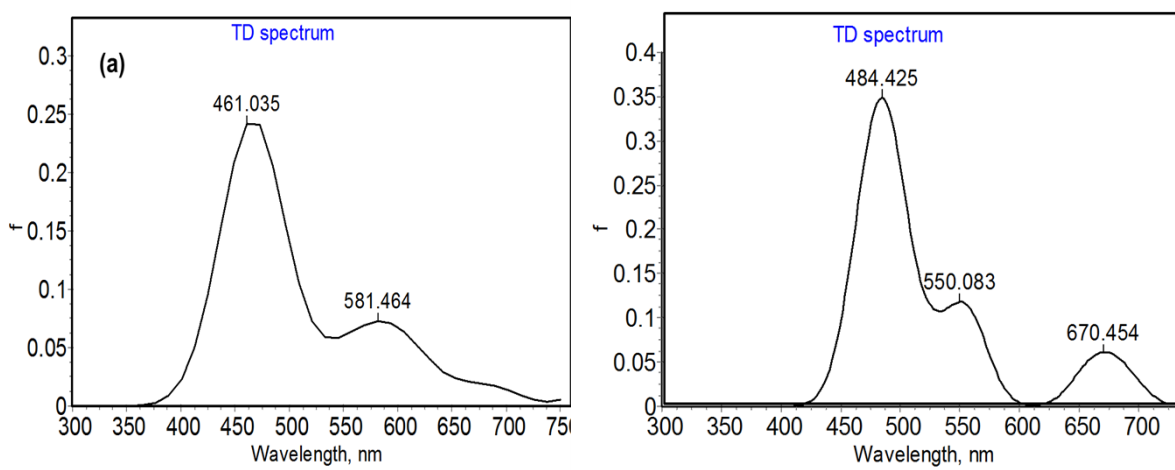


Figure S19. Theoretical UV-Visible spectra of (a) **4** and (b) **4•2CN⁻** obtained by TD-DFT calculations in gas phase.

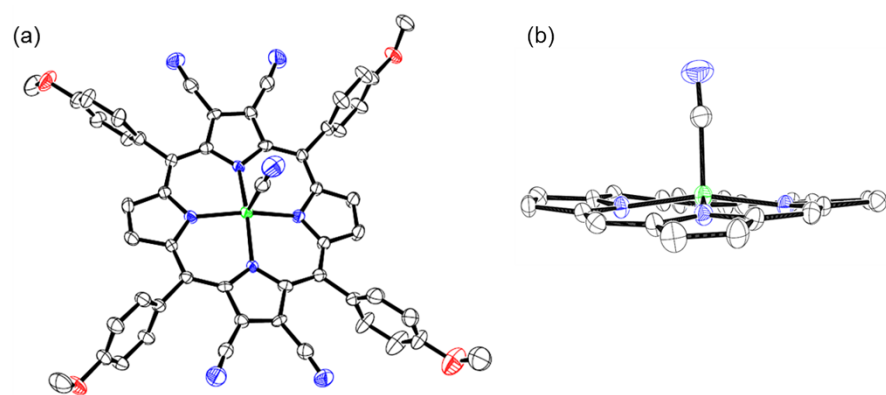


Figure S20. Single crystal X-ray structure of **3** with axial coordination of CN⁻ ion. The counter cation (tetrabutylammonium ion) was not shown for clarity.

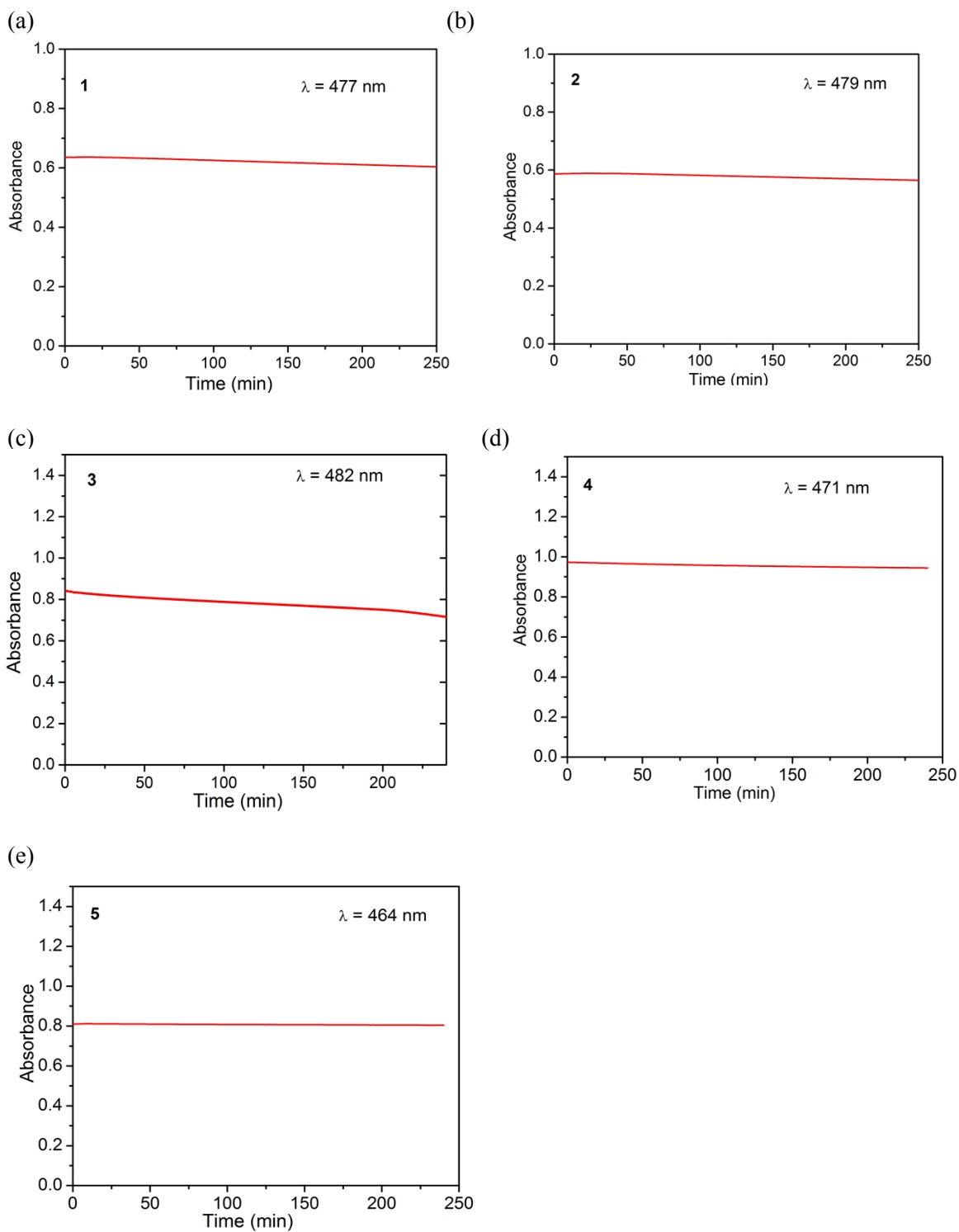


Figure S21. The time-dependent absorption changes of 1-5 after addition cyanide ions for 4 hours in toluene at 298 K.

Comment 1
Comment 2

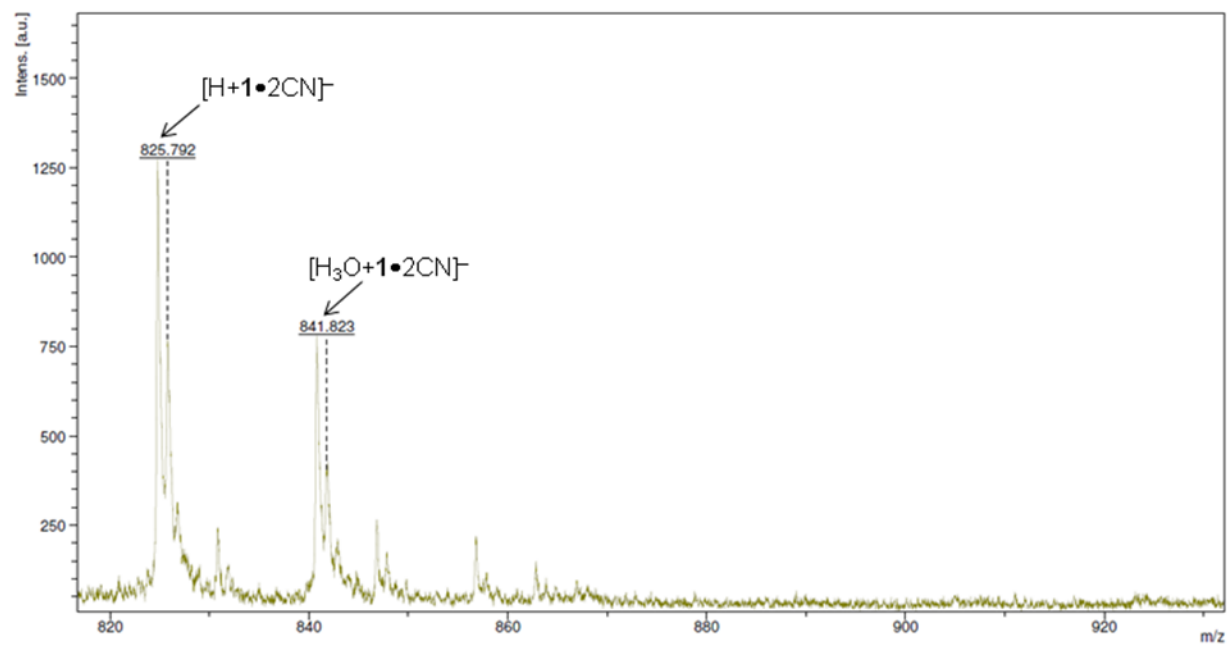


Figure S22. MALDI-TOF negative ion mode mass spectrum of **1** in presence cyanide ions using HABA matrix.

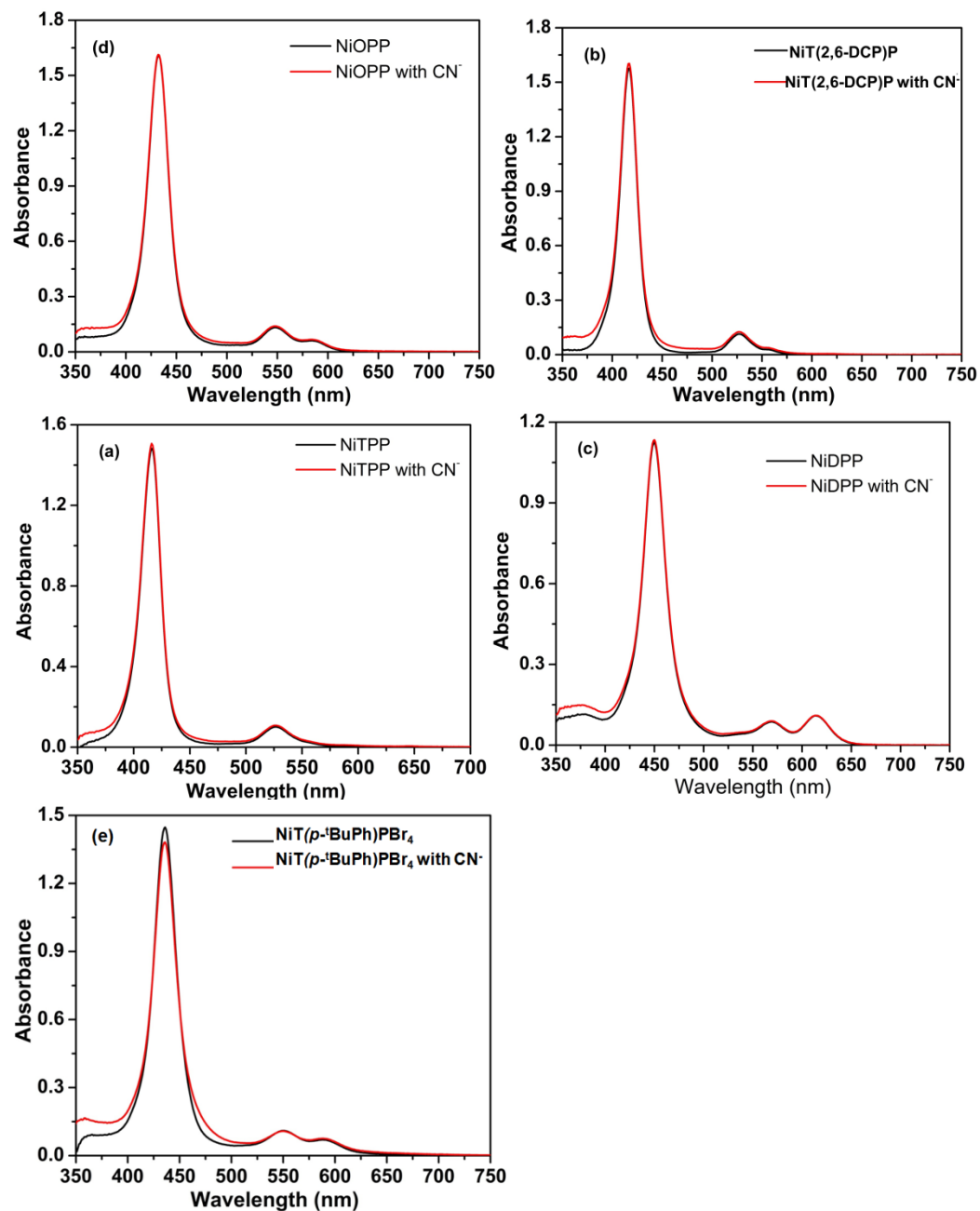


Figure S23. UV-Visible spectra of (a) *meso*-tetraphenylporphyrinato nickel(II) (NiTPP); (b) *meso-tetrakis*(2,6-dichlorophenyl)porphyrinato nickel(II) (NiT(2,6-DCP)P); (c) 2,3,5,7,8,10,12,13,15,17, 18,20-dodecaphenylporphyrinato nickel(II) (NiDPP); (d) 2,3,5,10,15,17,18,20-octaphenyl-porphyrinato nickel(II) (NiOPP); (e) *Meso-tetrakis*(*p*-butylphenyl)porphyrinato nickel(II) (NiT(*p*-*t*bu-ph)P) in toluene (black lines) at 298 K and then excess addition of [CN⁻] in toluene (red lines).

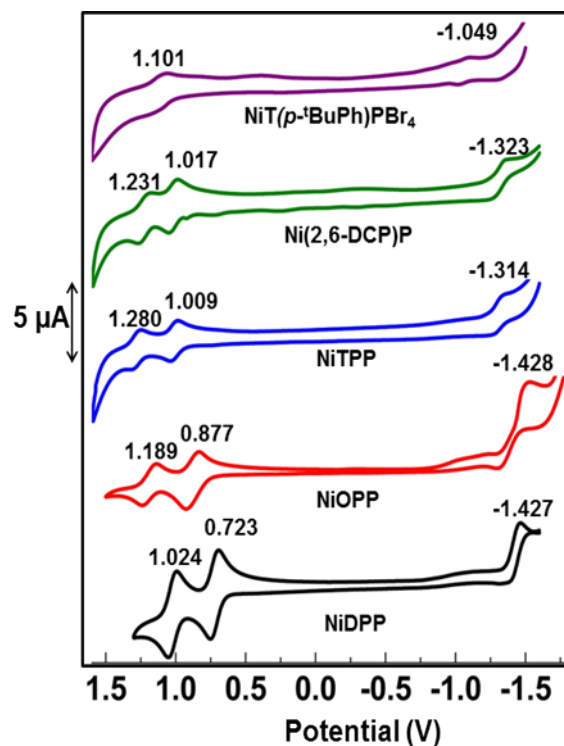


Figure S24. CVs of various planar and nonplanar Ni(II) porphyrins in CH_2Cl_2 at 298 K.

Table S5. Electrochemical redox data of various planar and nonplanar porphyrins in CH_2Cl_2 at 298 K.

Porphyrin	Oxidation (V)		Reduction (V)
	I	II	I
NiTPP	1.009	1.280	-1.314
NiOPP	0.877	1.189	-1.428
NiDPP	0.723	1.024	-1.427
NiT(2,6-DCP)P	1.017	1.231	-1.323
NiT(<i>p</i>-<i>t</i>BuPh)PBr₄	1.101	-	-1.049